ARTICLES

Local Crystal Structure around Manganese in New Potassium-Based Nanocrystalline Manganese Oxyiodide

Seong-Ju Hwang,[†] Chai-Won Kwon,[†] Josik Portier,[†] Guy Campet,*[,†] Hyo-Suk Park,[‡] Jin-Ho Choy,*[,‡] Pham V. Huong,[§] Masahiro Yoshimura,[||] and Masato Kakihana[||]

Institut de Chimie de la Matière Condensée de Bordeaux (ICMCB) du CNRS, 87 Av. du Dr. A. Schweitzer, 33608 Pessac, France, National Nanohybrid Materials Laboratory, School of Chemistry, Seoul National University, Seoul 151-747, Korea, Laboratoire de Physico-Chimie Moléculaire, Université Bordeaux I, 351 Cours de la Libération, 33405 Talence, France, and Department of Materials Science and Engineering, Tokyo Institute of Technology, 4259 Nagatsuta, Midori-ku, Yokohama 226, Japan

Received: July 13, 2001; In Final Form: January 17, 2002

A new nanocrystalline potassium-based lithium manganese oxyiodide has been prepared by using *Chimie Douce* route at room temperature. According to the electrochemical measurements, this nanocrystalline sample shows a large initial capacity up to ∼340 mAh/g at a constant current density of 0.2 mA/cm^2, which is much larger than that of sodium-based homologue. The X-ray diffraction analysis demonstrates that the amorphous character of the nanocrystalline compounds is maintained before and after chemical lithiation reaction. The local crystal structure around manganese in these materials has been determined by performing the combinative micro-Raman and X-ray absorption spectroscopy. From the Mn K-edge X-ray absorption near-edge structure and micro-Raman results, it becomes certain that manganese ions are stabilized in the rhombohedral layered lattice consisting of edge-shared MnO_6 octahedra, and the crystal symmetry is changed into a monoclinic symmetry upon reaction with *n*-BuLi. The Mn K-edge extended X-ray fine structure analysis reveals that the structural distortion caused by lithiation process is less significant for these nanocrystalline compounds than for the spinel lithium manganate. In this context, the great discharge capacity of the nanocrystalline materials is attributable for the pillaring effect of larger alkali metal ion than lithium ion, providing an expanded interlayer space available for Li insertion. In addition, the I L_I-edge X-ray absorption near-edge structure results presented here make it clear that iodine is stabilized as iodate species on the grain boundary or the surface of the nanocrystalline manganese oxyiodide, which helps to maintain the nanocrystalline nature of the present materials before and after Li insertion.

Introduction

Recently, special attention has been paid for lithium manganese oxides as promising cathode materials for lithium rechargeable batteries, which is due to the low toxicity, rich abundance, and low price of manganese.[1] In this context, various types of lithium manganates have been explored for the purpose of developing new cathode materials with better electrochemical performance.[2−4] However, most of lithium manganates experience a common structural modification to a spinel-type cation ordering in the course of electrochemical cycling.[5,6] This thermodynamically stable spinel phase has been well-known to suffer from capacity fading during repeated charge−discharge cycling.[1] The capacity loss of this cathode material is closely related to the structural transition from cubic spinel to tetragonal one, leading to a structural breakdown and to a formation of electronically isolated zones.[7] In fact, this sort of problem originating from the phase transition is considered to be more or less inevitable for well-crystallized lithium metal oxides. Such a speculation gives an impetus to develop amorphous phases as alternative cathode materials, since this type of compounds would be much more tolerable for the repeated Li insertion−deinsertion process. For example, very recently we have found that nanocrystalline spinel compound exhibits an enhanced electrochemical performance for 3 V region corresponding to Li insertion into 16c site in the spinel phase, which would be understood by the grafting mechanism of lithium on the surface of nanocrystalline material.[8] In addition, there have been some reports on nanocrystalline lithium manganese oxides showing superior electrochemical properties over well-crystalline homologues.[9−12] Among these nanocrystalline materials, sodium-based manganese oxyiodides possess a quite large discharge capacity and the best cyclability, and moreover their electrochemical performances can be improved by ball-milling process.[9] On the other hand, Whittingham, M. S. et al. reported

* To whom correspondence should be addressed.Guy Campet: Phone: +33-5-56-84-62-97. Fax: +33-5-56-84-27-61. E-mail: campet@icmcb.u-bordeaux.fr. Jin-Ho Choy: Phone: +82-2-880-6658. Fax: +82-2-872-9864. E-mail: jhchoy@plaza.snu.ac.kr.

[†] Institut de Chimie de la Matière Condensée de Bordeaux (ICMCB) du CNRS.

[‡] Seoul National University.

[§] Université Bordeaux I.

[||] Tokyo Institute of Technology.

10.1021/jp012704g CCC: $22.00
Published on Web 03/30/2002

that a potassium-based manganate with rhombohedral layered structure is more stable for electrochemical lithiation−delithiation reaction compared to sodium- or lithium-based ones.[13] Nonetheless, to our knowledge, there is no systematic study on potassium-based nanocrystalline manganese oxyiodide although it is worthwhile to probe the effect of alkali metal on the electrochemical properties of these nanocrystalline manganese oxyiodide. From the viewpoint of solid-state chemistry, it is also important to determine the local structure around manganese and the role of iodine species in understanding the mechanism of Li insertion in this nanocrystalline material. However, it is quite difficult to probe the local cation ordering of nanocrystalline compounds because of their X-ray amorphous character. In our recent papers, it was demonstrated that a combination of micro-Raman and X-ray absorption spectroscopy (XAS) is very effective in probing the local atomic structure of electrode materials with poor crystallinity as well as in examining the effect of Li insertion−deinsertion process on the chemical bonding character of these compounds.[5,14,15]

In this work, we have prepared a new potassium-based nanocrystalline manganese oxyiodide and characterized its physicochemical properties in comparison with those of sodium-based homologue. In addition, an attempt has been made to determine the local geometric and electronic structures around manganese before and after chemical lithiation by using micro-Raman and Mn K-edge XAS analyses.[16] The chemical bonding characters of iodine species in these nanocrystalline materials have also been studied by performing the X-ray absorption near-edge structure (XANES) analysis at I L_I-edge.

Experimental Section

Sample Preparation. The nanocrystalline A−Li−Mn−O−I (A = K and Na) samples were prepared by reacting the aqueous solution of $KMnO_4$ or $NaMnO_4$•H_2O with 1.5 equiv LiI at room temperature, similar to the previously reported *Chimie Douce* method.[9,10] The mixed solution was maintained for 1 day under constant stirring. The resulting precipitate was washed with water and was dried at 130 °C in a vacuum. The chemical lithiation reaction for these amorphous samples was carried out by reacting them with 1.6 M *n*-BuLi in hexane for 48 h. Prior to the physicochemical characterization, the lithiated samples were washed thoroughly with hexane and ethanol and were dried in a vacuum.

Sample Characterization. The crystal structures of A−Li−Mn−O−I (A = K and Na) and their chemically lithiated products were studied by X-ray diffraction (XRD) measurement using Ni-filtered Cu Kα radiation with a graphite diffracted beam monochromator. The chemical compositions of these samples were determined by using atomic absorption (AA) spectrometry, inductive coupled plasma (ICP) spectrometry, and electron probe for microanalysis (EPMA). The water contents were estimated by performing thermogravimetric analysis (TGA) under O_2 flow. The weight losses of ∼3% and ∼6% up to ∼150 °C are observed for the Na- and K-based nanocrystals, respectively, indicating that these materials possess about 0.2−0.4 mole water per unit formula.[13] The electrochemical measurements were performed with the cell configuration of Li/1M $LiPF_6$ in EC:DEC (50:50 v/v)/composite cathode, which was assembled in a drybox. The composite cathode was prepared by mixing thoroughly the active A−Li−Mn−O−I (A = K and Na) material (20 mg, 70 wt %) with 25 wt % of acetylene black and 5 wt % of PTFE (poly(tetrafluoroethylene)). All the experiments were carried out in a galvanostatic mode with Arbin BT 2043 multichannel galvanostat/potentiostat in the voltage range of 1.5−4.3 V at the constant current densities of 0.2 and 0.5 mA/cm^2 (10 and 25 mA/g).

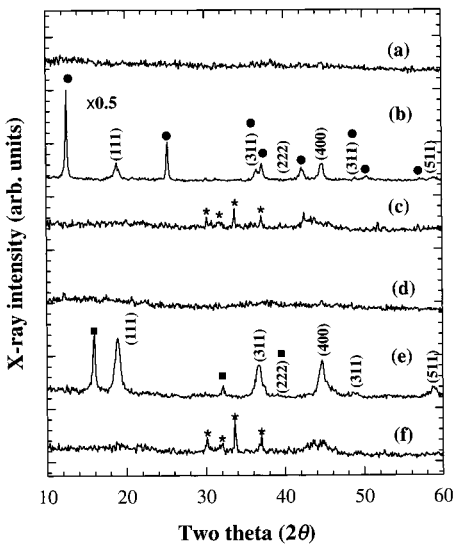

Figure 1. X-ray diffraction patterns of (a) nanocrystalline K−Li−Mn−O−I compound and its derivatives (b) after the heat treatment at 600 °C and (c) after lithiation, together with (d−f) the corresponding data of Na-homologues. In (b) and (e), the indexed reflections are assigned on the basis of cubic spinel structure, and the circle and square symbols represent the reflections from K_xMnO_2•yH_2O and $Na_{0.7}MnO_2$ phases, respectively. The asterisk symbols in (c) and (f) denote the peaks originating from $LiOH$•H_2O.

Micro-Raman Spectroscopy. The micro-Raman spectra presented here were recorded on a Dilor-Omars microspectrometer coupled with an optical microscope (spatial resolution of 1 μm^2) and an intensified 1024-channel photodiode array detector. The 514.5-nm line from an argon ion laser Spectra Physics model 2016 was used as an excitation source. All the present spectra were measured by backscattering from the freshly fractured surfaces of the pellet or from the powdered sample. To prevent possible thermal damage of the samples, the power of incident laser light was maintained at less than 1 mW. After each measurement, the sample surface was thoroughly checked to remove the possibility of spectral modification caused by surface degradation.

X-ray Absorption Measurement. The XAS experiments were performed for the nanocrystalline A−Li−Mn−O−I (A = K and Na) compounds and their lithiated derivatives by using the extended X-ray absorption fine structure (EXAFS) facility installed at the beam line 7C at the Photon Factory in Tsukuba.[17] The XAS data were collected at room temperature in a transmission mode using gas-ionization detectors. All the present spectra were calibrated by measuring the spectra of Mn metal foil and KI. The data analysis for the experimental spectra was carried out by the standard procedure as reported previously.[5]

Results and Discussion

Powder XRD and Chemical Analyses. The powder XRD patterns of as-prepared A−Li−Mn−O−I (A = K and Na) compounds are shown in Figure 1, together with those of their heated and lithiated products. No distinct reflection can be observed for the nanocrystalline samples heated at 130 °C in vacuum. After the heat-treatment at 600 °C, an amorphous phase is changed into a mixed crystalline phase, that is, a mixture of rhombohedral layered K_xMnO_2[18] and cubic-spinel $Li_{1+y}Mn_{2-y}O_4$ for the potassium-based nanocrystal and a mixture of $Na_{0.7}MnO_2$[19] and cubic-spinel $Li_{1+y}Mn_{2-y}O_4$ for the sodium-based

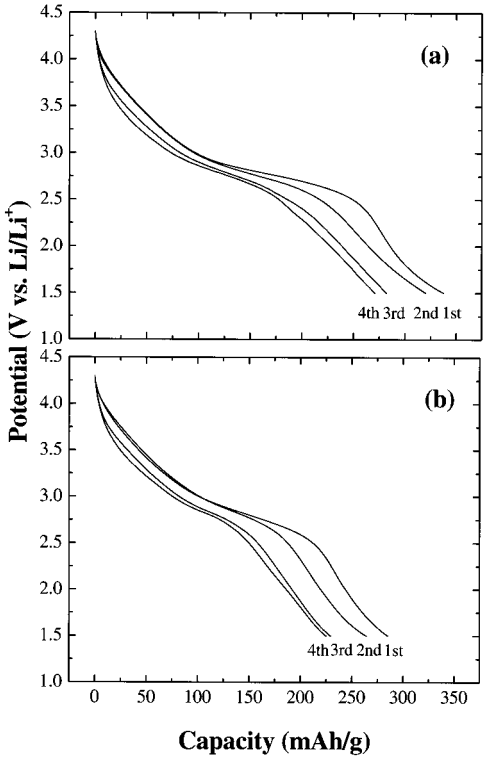

Figure 2. Discharge potential profiles of the nanocrystalline A−Li−Mn−O−I compounds with A = (a) K and (b) Na. The electrochemical measurements were carried out in the potential range of 1.5−4.3 V with the applied current density of 0.2 mA/cm^2.

TABLE 1: Chemical Formulas of Nanocrystalline Manganese Oxyiodides and Their Lithiated Derivatives

sample	as-prepared	lithiated
K−Li−Mn−O−I	$Li_{0.54}K_{0.31}MnO_{2.5-\delta}I_{0.10}$	$Li_{2.45}K_{0.34}MnO_{2.5-\delta}I_{0.13}$
Na−Li−Mn−O−I	$Li_{0.52}Na_{0.62}MnO_{2.5-\delta}I_{0.07}$	$Li_{2.48}Na_{0.79}MnO_{2.5-\delta}I_{0.08}$

nanocrystal. In the lithiated derivatives, there is no XRD peak related to the crystalline lithium manganate, except several weak reflections corresponding to a small amount of lithium hydroxide hydrate formed by a reaction with *n*-BuLi and water of the samples. This finding indicates that the amorphous structure of the present nanocrystalline manganese oxyiodides is highly tolerable for Li insertion reaction.

The chemical formula of the nanocrystalline A−Li−Mn−O−I (A = K and Na) compounds and their lithiated derivatives estimated from AA, ICP, and EPMA analyses is summarized in Table 1. The concentration of alkali metal ion is determined to be smaller for the potassium-based nanocrystal than for the sodium-based one, whereas the iodine content is larger for the former compared to the latter. As listed in Table 1, the lithiation process results in the incorporation of about two moles of lithium ions per unit formula commonly for both nanocrystalline materials. This reflects their greater ability to accommodate lithium ions compared to well-crystallized electrode materials such as $LiMn_2O_4$ spinel, even though a fraction of lithium ions are consumed for the reaction with the sample water, leading to the formation of lithium hydroxide.

Electrochemical Performance. The cycling characteristics of the nanocrystalline A−Li−Mn−O−I (A = K and Na) compounds have been examined to probe the effect of alkali metal on the electrochemical performance of the lithium manganese oxyiodides. Since both pristine materials possess an open circuit potential of ∼3.4 V (vs Li/Li$^+$), the electrochemical cycling starts with the first charge process up to 4.3 V. The

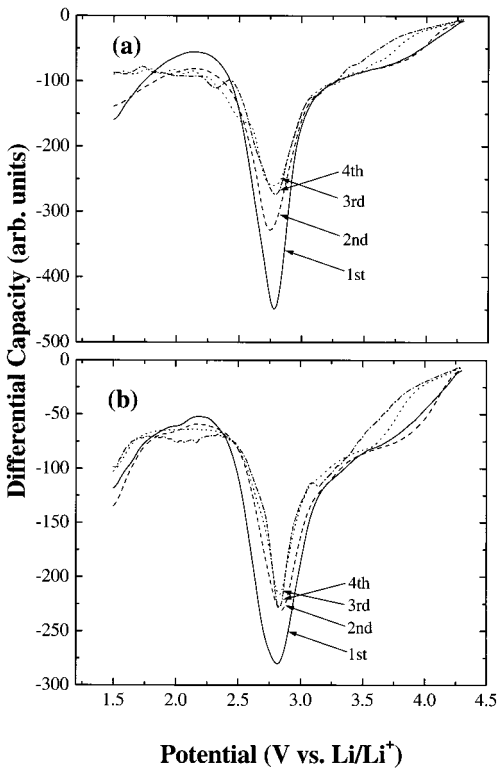

Figure 3. Differential capacity profiles of the nanocrystalline A−Li−Mn−O−I compounds with A = (a) K and (b) Na. The electrochemical measurements were carried out in the potential range of 1.5−4.3 V with the applied current density of 0.2 mA/cm^2.

discharge potential profiles of the nanocrystalline A−Li−Mn−O−I (A = K and Na) compounds measured at a constant current density of 0.2 mA/cm^2 are plotted in Figure 2. For both compounds, a small capacity of ∼110 mAh/g corresponding to the oxidation of trivalent manganese ions is commonly observed (not shown in the figure), which is much smaller than the capacity of the following discharge process. This underlines that the electrochemical activity of these manganese oxyiodides is attributed mainly to the insertion of lithium ion from Li anode rather than to the reinsertion of lithium ions which already exist in the as-prepared materials. Both nanocrystals show nearly identical curve shape, which is very close to that of the previously reported amorphous manganese dioxide,[9−11] confirming the amorphous character of the present manganese oxyiodides. The observed smooth decrease of potential during discharge process is a characteristic of nanocrystalline electrode materials such as SnO_2, Fe_2O_3, and so forth.[20,21] This can be explained by the fact that the existence of surface defects or surface dangling bonds in nanocrystalline materials gives rise to the formation of many sub-bands between valence and conduction bands, leading to a smooth change of Fermi energy and hence a slow potential change.[8] In comparison with the sodium-based manganese oxyiodide, the potassium-based one shows a greater discharge capacity for each cycle. For a more accurate inspection of discharge behaviors, the differential capacity profiles of the nanocrystalline A−Li−Mn−O−I (A = K and Na) compounds are presented in Figure 3. As the cycle proceeds, no significant change in curve shape except a slight depression of the peak at ∼2.7 V can be observed for both compounds, which suggests that the electrochemical discharge−charge process does not induce any marked structural transition in these nanocrystalline materials. However, the present nanocrystals commonly show a significant capacity fading, which is fairly contrasted with the previous report on

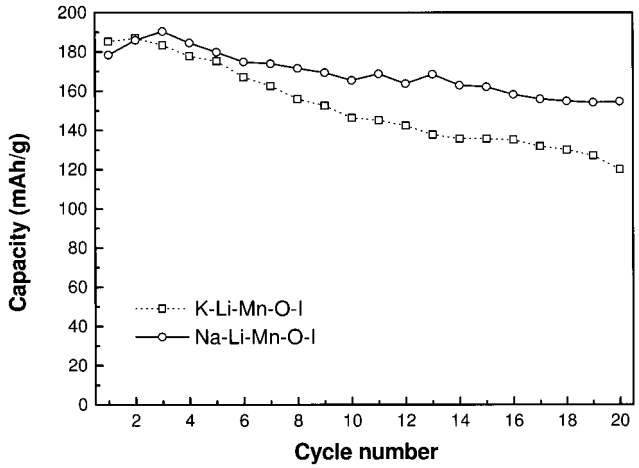

Figure 4. Discharge capacities of the nanocrystalline A−Li−Mn−O−I compounds with A = K (squares) and Na (circles). The electrochemical measurements were carried out in the potential range of 1.5−4.3 V with the applied current density of 0.5 mA/cm^2.

the sodium-based materials prepared in acetonitrile solvent.[9] This may be attributed not to the structural transition but to the presence of water leading to the formation of LiOH and HF via the reaction with Li anode and electrolyte, respectively. In this context, now we are trying to prepare potassium-based nanocrystal in nonaqueous solvent and to examine the effect of ball milling on its electrochemical property, with a view to improving the cyclability and discharge capacity of this promising nanocrystalline material. On the other hand, we have also measured the electrochemical performances of the present nanocrystalline samples up to 20 cycles with a higher current density of 0.5 mA/cm^2, to examine the long-term cycling characteristics as well as to probe the effect of current density. As presented in Figure 4, the potassium-based phase shows the high initial discharge capacity of 185 mAh/g with a notable capacity decrease to 120 mAh/g after the 20th cycle, whereas the sodium-based one exhibits a better capacity retention from 178 mAh/g at the first cycle to 155 mAh/g at the 20th cycle. This is surely contrasted with the results obtained with the lower current density of 0.2 mA/cm^2. Such different long-term cycle characteristics of these nanocrystals are suggested to originate from their dissimilar water contents or from the contribution of other chemical species such as Na/K or iodine to discharge capacity. However, it is quite difficult to conclude here the origin of the observed electrochemical behavior of the present nanocrystals, since there are so many factors to be considered influencing the long-term cycling performance. To answer this question, now we are performing the detailed electrochemical measurements with various experimental conditions. In this context, here we limit our further discussion to why the potassium-based phase shows a greater "initial" discharge capacity than the sodium-based one. In fact, prior to the electrochemical measurements, we expected that the potassium-based compound possesses inferior initial discharge capacity to the sodium-based one, judging from the heavier atomic weight of potassium compared to sodium. But this is not true for the nanocrystalline materials presented here. To understand such an unexpected finding, we have examined the local structure around manganese in both nanocrystalline compounds by performing micro-Raman and XANES/EXAFS tools complementarily.

Mn K-Edge XANES Analysis. The Mn K-edge XANES spectra of the pristine nanocrystalline A−Li−Mn−O−I (A = K and Na) compounds and their lithiated derivatives are

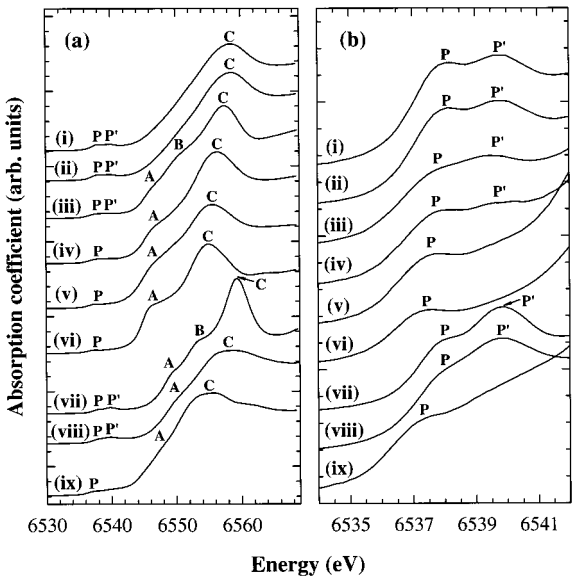

Figure 5. (a) Mn K-edge XANES spectra for the nanocrystalline A−Li−Mn−O−I compounds with A = (i) K and (ii) Na and (iv−v) their lithiated derivatives, in comparison with the references (iii) cubic spinel $LiMn_2O_4$, (vi) tetragonal spinel $Li_2Mn_2O_4$, (vii) λ-MnO_2, (viii) nanocrystalline manganese oxide, and (ix) Mn_2O_3. The magnified spectra for preedge region are presented in (b).

illustrated in Figure 5a, in comparison with the reference spectra of cubic spinel $LiMn_2O_4$, tetragonal spinel $Li_2Mn_2O_4$, λ-MnO_2, nanocrystalline manganese oxide,[22,23] and Mn_2O_3. The position of the edge jump for the pristine manganese oxyiodides is a little bit higher than that for $LiMn^{+IV}Mn^{+III}O_4$ but slightly lower than that for λ-$Mn^{+IV}O_2$, which indicates that manganese ions in these materials have an average valence state of $>+3.5$. Actually, the sodium-based manganese oxyiodide has been reported to possess the average Mn oxidation state of about $+3.8$.[9] In the lithiated manganese oxyiodides, the edge position is rather in accordance with that of tetragonal spinel $Li_2Mn^{+III}{}_2O_4$, confirming the reduction of manganese ions after the *n*-BuLi-treatment. In the preedge region, all the spectra presented here show small preedge peaks (denoted P and P′), which are assigned as the transitions from the core 1s level to unoccupied 3d states. Even though they are not allowed by the electronic dipolar selection rule, $\Delta l = \pm 1$, the preedge peaks could be discerned either because of quadrupole-allowed transitions or because of the mixing of 4p and 3d states.[5] In this context, the weak intensity of these features suggests that all the manganese ions in the samples under investigation are stabilized in octahedral site with an inversion center. The position and shape of these preedge peaks are well-known to be closely related to the oxidation state of the absorbing ion and the local arrangement of backscattering ions, respectively.[5] As can be seen clearly from Figure 5b, the relative energies of the preedge peaks are wholly consistent with the order of the main-edge positions. It is also evident that the spectral shape of preedge features in all the samples presented here can be classified into two groups; two preedge peaks P and P′ are discernible for some materials containing considerable amount of tetravalent manganese ions, whereas only one feature P at lower energy can be observed for the others with trivalent manganese ions. In fact, the latter characteristic preedge feature for trivalent manganese compounds can be interpreted as a result of the splitting of t_{2g} and e_g energy levels modified by Jahn−Teller deformation.[24] For the nanocrystalline manganese oxyiodides under investigation, both the pristine materials exhibit

nearly the same spectral features in preedge region, whereas there are marked spectral differences between the corresponding lithiated derivatives. That is, the lithiation reaction gives rise to a smaller change in the preedge features of the potassium-based nanocrystal compared to the sodium-based one, which suggests that the Jahn−Teller deformation of the MnO_6 octahedra is smaller in the former. In the main-edge region, there are some peaks (denoted A, B, and C), which are assigned as the dipole-allowed transitions from the core 1s level to unoccupied 4p states. In contrast to the well-crystallized $LiMn_2O_4$ and λ-MnO_2,[25] both the pristine nanocrystalline compounds do not show the fine features A and B in this region, which is attributed to the absence of long-range crystal order. This finding is well consistent with the recent XANES study for Na-based nanocrystal.[26] On the contrary, a distinct peak A is clearly observed for both the lithiated derivatives as well as for tetragonal spinel $Li_2Mn_2O_4$, although its spectral weight is weaker for the former than for the latter. Since the strong peak A is an indicator of trivalent manganese ion stabilized in the Jahn−Teller distorted octahedra,[5] the observed weak intensity of peak A indicates that the Jahn−Teller deformation around manganese is less prominent for the nanocrystalline manganese oxyiodide than for the well-crystallized tetragonal spinel, as reported recently.[26] Moreover, a closer inspection on the present XANES spectra reveals that K-based nanocrystal exhibits smaller intensity of peak A than Na-based one, which is well correlated with less prominent change of preedge features after lithiation in the former. On the other hand, an intense and sharp peak C appears commonly for all the nanocrystalline manganese oxyiodides including the lithiated derivatives as well as for the spinel-structured compounds. Considering the fact that the intensity of this peak is proportional to the relative concentration of edge-shared MnO_6 octahedra with respect to corner-shared one,[27] it can be supposed that the crystal structure of nanocrystalline manganese oxyiodides consists of edge-shared MnO_6 octahedra like spinel-structured compounds. In contrast, only a broader and less intense peak C can be discerned for another nanocrystalline manganate without iodine and potassium species (sample viii in Figure 5), indicating this compound has the intergrowth structure of edge- and corner-shared MnO_6 octahedra. On the basis of this finding, it can be supposed that iodine and potassium ions may act as stabilizers for edge-shared MnO_6 network. It has been known that there are some kinds of lithium manganate phases such as spinel $LiMn_2O_4$, layered $LiMnO_2$, and so forth, whose crystal structures constitute with edge-shared MnO_6 octahedra. However, on the basis of the present Mn K-edge XANES results, it is very difficult to determine conclusively the local structure around manganese in the nanocrystalline manganese oxyiodides. To solve this problem, we have applied micro-Raman spectroscopy.

Micro-Raman Spectroscopy. The Raman spectra of the nanocrystalline A−Li−Mn−O−I (A = K and Na) compounds are represented in Figure 6, together with the reference spectra of rhombohedral layered $LiCoO_2$, cubic spinel $LiMn_2O_4$, monoclinic layered $LiMnO_2$, and tetragonal spinel $Li_2Mn_2O_4$. As predicted by the factor group analysis, the rhombohedral $LiCoO_2$ compound exhibits two A_{1g} and E_g phonon lines at 486 and 596 cm^{-1}, whereas three Raman peaks corresponding to Raman-active $2A_g + B_g$ modes are observed for the layered $LiMnO_2$ oxide at 422, 481, and 603 cm^{-1}.[15,28] In the spinel-structured compounds, a larger number of Raman peaks appear because of their complex crystal structure. As shown in Figure 6, the present cubic spinel $LiMn_2O_4$ sample shows four Raman peaks at 270, 340, 454, and 631 cm^{-1}, which are assigned as $2T_{2g}$,

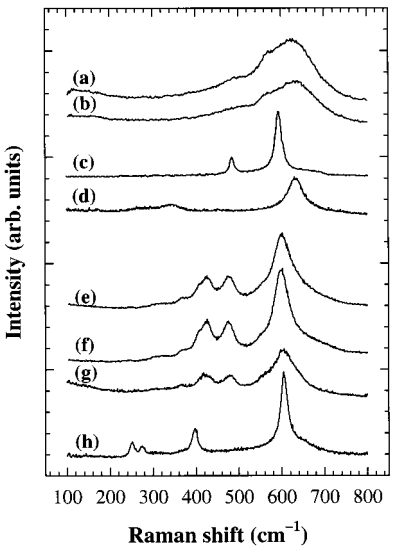

Figure 6. Micro-Raman spectra for the nanocrystalline A−Li−Mn−O−I compounds with A = (a) K and (b) Na and (e−f) their lithiated derivatives, in comparison with the references (c) rhombohedral layered $LiCoO_2$, (d) cubic spinel $LiMn_2O_4$, (g) monoclinic layered $LiMnO_2$, and (h) tetragonal spinel $Li_2Mn_2O_4$.

E_g, and A_{1g} mode, respectively, whereas four characteristic phonon lines can be detected for the tetragonal spinel phase in the frequency range 200−650 cm^{-1}. The Raman spectrum of tetragonal spinel $Li_2Mn_2O_4$ can be clearly distinguished from that of monoclinic layered $LiMnO_2$, even though both the lithium manganates show almost the same XRD patterns.[29] This is because the Raman spectrum is strongly dependent on the crystal symmetry rather than on the structure factor. In this regard, the Raman spectroscopy enables us to easily identify various lithium manganate phases with closely related crystal structures such as layered $LiMnO_2$ (*C*2/*m*), tetragonal spinel $Li_2Mn_2O_4$ (*I*4$_1$/*amd*), orthorhombic $LiMnO_2$ (*Pmnm*), and so forth.[15] In the nanocrystalline manganese oxyiodides, two very broad features are discernible around 490 and 630 cm^{-1}. Considering that the nanocrystalline nature and the mixed Mn oxidation state of the present manganese oxyiodides are surely responsible for the very broad Raman feature, the Raman spectra of these nanocrystals are somewhat similar to that of rhombohedral $LiCoO_2$ rather than that of spinel $LiMn_2O_4$. However, the considerable broadness of features makes it very difficult to definitively determine the local structure of nanocrystalline materials on the basis of the present Raman spectra. In this regard, we have also examined the Raman spectra of lithiated manganese oxyiodides, since the lithiation usually increases the signal-to-noise (S/N) ratio of Raman data by depressing the electrical conductivity. As can be seen clearly from Figure 6, there is remarkable spectral consistency between the nanocrystalline materials and the monoclinic layered $LiMnO_2$, highlighting that the lithiated derivatives possess the layered structure with monoclinic distortion. Generally the reduction of Mn oxidation state induces a Jahn−Teller distortion around manganese, giving rise to a structural transition from rhombohedral layered to monoclinic layered, or from cubic spinel to tetragonal spinel. Moreover, it is impossible to change from a spinel structure to a layered one during lithiation process, since the spinel structure is thermodynamically more stable than the layered one. In this regard, we can conclude that the manganese ion in nanocrystalline manganese oxyiodide crystallizes locally in rhombohedral layered cation ordering not in the spinel-type one, and the lithiation reaction results in a local structural change into monoclinic layered structure.

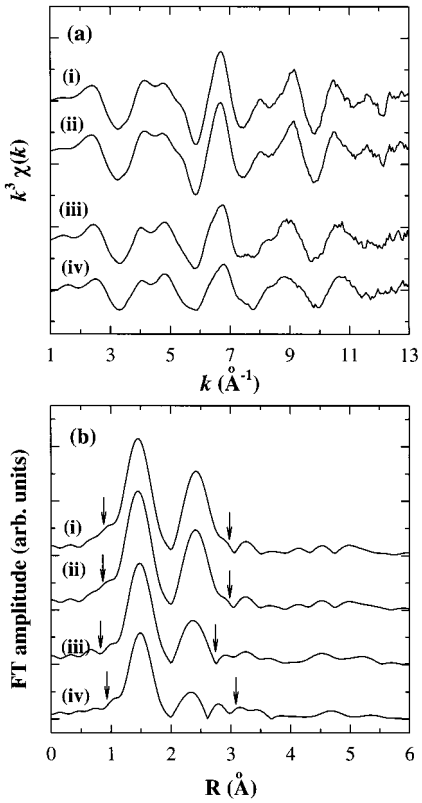

Figure 7. (a) k^3-weighted Mn K-edge EXAFS spectra and (b) their Fourier transforms for the nanocrystalline A−Li−Mn−O−I compounds with A = (i) K and (ii) Na and (iii−iv) their lithiated derivatives. The range over which the Fourier filtering has been made is shown by the arrows.

Mn K-Edge EXAFS Analysis. The local structural variation of the nanocrystalline A−Li−Mn−O−I (A = K and Na) compounds upon chemical lithiation process has been examined quantitatively using Mn K-edge EXAFS spectroscopy. The k^3-weighted Mn K-edge EXAFS spectra for the nanocrystalline A−Li−Mn−O−I (A = K and Na) compounds and their lithiated derivatives are represented in Figure 7a and the corresponding Fourier transforms (FTs) in Figure 7b. As can be seen from Figure 7a, the overall spectral features of the EXAFS oscillation of the pristine nanocrystalline compounds are quite similar to each other, indicating the same local structure around manganese in both compounds. On the other hand, the lithiation process gives rise to a spectral change in EXAFS oscillation which is less prominent for K-based material than for Na-based one, as observed in XANES region. In the FT diagrams (Figure 7b), the nanocrystalline manganese oxyiodides exhibit two intense FT peaks at ∼1.5 and ∼2.5 Å, which are attributed to the (Mn−O) and (Mn−Mn) shells, respectively. Upon lithiation reaction, the FT peaks become depressed especially for (Mn−Mn) shell, which can be understood from the fact that the Jahn−Teller distortion around Mn causes a damping of EXAFS signal. However, in contrast to the previously reported results for the spinel phase,[25,30] the splitting of FT peaks corresponding to (Mn−Mn) shells induced by lithiation is not obvious for the present nanocrystalline compounds, which is well correlated with the XANES results.[26] Between both lithiated nanocrystals, the splitting of (Mn−Mn) shells is more well-resolved for Na-based material than for K-based one. These findings can be regarded as further evidence for the excellent endurance of the amorphous character of these nanocrystalline materials during Li insertion reaction, especially for the K-based nanocrystal. The peaks at 4−6 Å originated from the multiple scattering paths with focusing effect are nearly suppressed in the present compounds, in contrast to the well-crystalline $LiMnO_2$ and $LiMn_2O_4$ ones.[5,25] This confirms the nanocrystalline nature of the present manganese oxyiodides. To determine the structural parameters such as coordination number (CN), bond distance (R), and Debye−Waller factor (σ^2), these FT peaks were isolated by inverse Fourier transform to a k space and then were curve-fitted. In light of micro-Raman results, we have tried to reproduce the spectra of nanocrystalline manganese oxyiodides and their lithiated derivatives on the basis of the crystal structures of rhombohedral layered and monoclinic layered phases, respectively, in such a way that we were able to get reasonable fitting results.[31] The best fitting results are compared to the experimental $k^3\chi(k)$ Fourier filtered data in Figure 8, and the obtained structural parameters are listed in Table 2. While the manganese ion in the nanocrystalline A−Li−Mn−O−I (A = K and Na) compounds is stabilized in a regular MnO_6 octahedron with six neighboring oxygen ions at the same distance, the manganese ion in the lithiated derivatives exists in a Jahn−Teller distorted MnO_6 octahedra, as supposed from micro-Raman study. Moreover, the average (Mn−O) and (Mn−Mn) bond distances of the nanocrystalline materials are found to be elongated by lithiation reaction, confirming the decrease of Mn oxidation state after reaction with *n*-BuLi. In addition, the coordination numbers are determined to be smaller

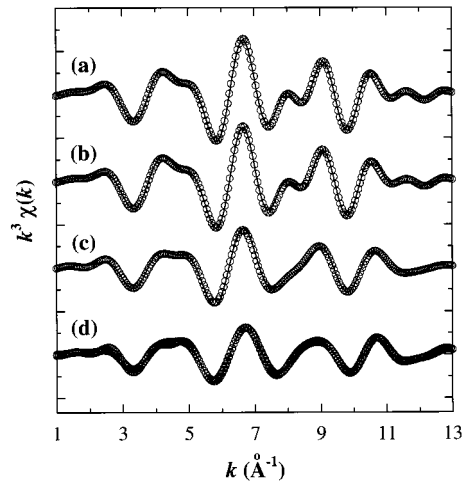

Figure 8. Fourier filtered Mn K-edge EXAFS spectra for the nanocrystalline A−Li−Mn−O−I compounds with A = (a) K and (b) Na and (c−d) their lithiated derivatives. The solid lines and empty circles represent the fitted and experimental data, respectively.

TABLE 2: Results of Nonlinear Least-Squares Curve-Fitting Analysis for the Mn K-edge EXAFS Spectra of Nanocrystalline Manganese Oxyiodides and Their Lithiated Derivatives

sample	bond	CN[a]	R (Å)	σ^2 (10^{-3} × Å^2)
K−Li−Mn−O−I	(Mn−O)	6.0	1.90	4.89
	(Mn−Mn)	4.2	2.86	6.22
Na−Li−Mn−O−I	(Mn−O)	6.0	1.90	4.95
	(Mn−Mn)	4.3	2.85	6.91
	(Mn−O_{eq})	4	1.90	3.21
Lithiated	(Mn−O_{ax})	2	2.33	10.60
K−Li−Mn−O−I	(Mn−Mn)	1.4	2.87	2.82
	(Mn−Mn)	2.8	3.02	9.99
	(Mn−O_{eq})	4	1.90	4.08
Lithiated	(Mn−O_{ax})	2	2.27	15.31
Na−Li−Mn−O−I	(Mn−Mn)	1.4	2.83	5.73
	(Mn−Mn)	2.8	3.02	15.11

[a] While the coordination numbers for (Mn−O) shells are fixed to the crystallographic values, those for (Mn−Mn) shells are set as variables in the curve-fitting analyses.

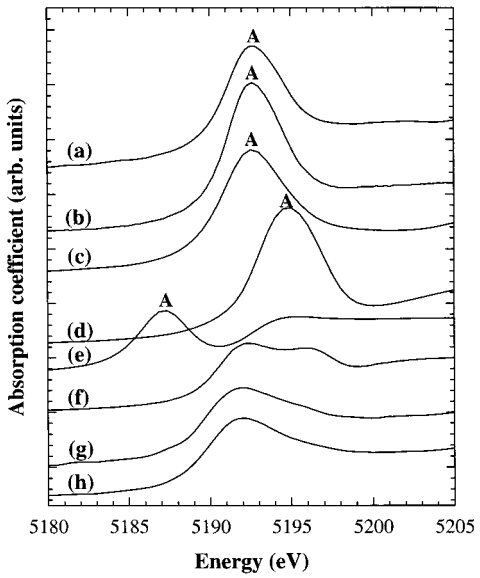

Figure 9. I L_I-edge XANES spectra for the nanocrystalline A−Li−Mn−O−I compounds with A = (a) K and (b) Na and (g−h) their lithiated derivatives, in comparison with the references (c) KIO_3, (d) KIO_4, (e) I_2, and (f) KI.

for (Mn−Mn) shells than for (Mn−O) shells, which reflects the nanocrystalline nature of the present samples leading to an incomplete coordination of manganese by distant shells.

I L_I-Edge XANES Analysis. As described in the Mn K-edge XANES section, another type of nanocrystalline manganate without iodine and potassium species crystallizes with edge- and corner-shared network of MnO_6 octahedra, in contrast to the present manganese oxyiodides. In this regard, it is a very interesting question what the role of iodine is. To give an answer to this question, we have studied the chemical bonding character of iodine species by performing I L_I-edge XANES analysis. The I L_I-edge XANES spectra of the nanocrystalline manganese oxyiodides and their lithiated derivatives are presented in Figure 9, in comparison with the reference spectra of KI, I_2, KIO_3, and KIO_4. All the reference spectra except for KI exhibit a characteristic white line (WL) peak at around 5185−5195 eV, which is ascribed to the transition from the 2s core level to the unoccupied 5p state.[32] Since the intensity of this WL feature is dependent on the density of the unoccupied 5p final state, the most intense peak is discernible for both KIO_3 and KIO_4 references having completely empty I 5p orbitals. On the contrary, this 2s → 5p transition is not possible for KI because of the full occupancy of I 5p orbital. In the pristine nanocrystalline materials, this WL peak shows almost the same position and intensity as the reference KIO_3, which indicates that the iodate species is stabilized in nanocrystalline manganate oxyiodides, as reported very recently.[26] There are two possibilities about the site of IO_3^- cluster in these nanocrystalline compounds; one is the interlayer site and the other is the grain boundary or the sample surface. As shown in Figure 9, a notable depression of peak A upon lithiation can be observed for both nanocrystalline materials, suggesting that most of iodate ion is reduced to a negatively charged iodide ion. Considering the electrostatic repulsion between iodide and oxide anions, it is impossible for iodide ion to exist in the interlayer octahedral site of rhombohedral layered lattice. However, the elemental analyses reveal that there still remain lots of iodine species after lithiation, which implies that most of iodine species in nanocrystalline manganese oxyiodide is located in the grain boundary or on the surface. Since the iodate ion stabilized in the grain boundary prevents an effective crystal growth of lithium manganese oxide grains, it would help to maintain the nanocrystalline nature of this material before and after Li insertion.

Summarizing the present experimental findings, it is evident that manganese ion in the present nanocrystalline compounds is stabilized in the rhombohedral layered-type local structure, which is maintained by the presence of alkali metal pillar rather than by the existence of iodate cluster in interlayer space. In this context, a greater initial discharge capacity of K-based nanocrystal compared to Na-based one is interpreted as a result of the expanded interlayer spacing sustained by larger potassium ion, giving a better ability to accommodate the lithium ion in the interlayer space.

Conclusion

In this study, an attempt has been made not only to determine the local structure of manganese in the nanocrystalline electrode materials but also to probe the effects of Li insertion on the atomic and electronic structures of these compounds by performing systematic micro-Raman and XAS analyses. The electrochemical measurements demonstrate that a newly prepared potassium-based lithium manganese oxyiodide shows a great initial discharge capacity of ∼340 mAh/g at 0.2 mA/cm^2, which is larger than that of sodium-based homologue. According to the XRD analysis, the amorphous nature of the present samples is maintained before and after lithiation reaction. The Mn K-edge XANES and micro-Raman results reveal that the manganese ion is stabilized in the rhombohedral layered lattice, and the crystal symmetry is changed into a monoclinic symmetry upon lithiation reaction. Despite layered local crystal structure, the present nanocrystalline materials exhibit no significant change in discharge potential profiles during lithium insertion−extraction process, which is surely contrasted with the layered $LiMnO_2$ phase with well-crystalline structure showing a structural transition to spinel-type cation ordering. This can be regarded as evidence of the better structural stability of nanocrystalline materials with respect to well-crystalline ones. The Mn K-edge EXAFS analysis confirms that the structural distortion is less prominent for the nanocrystalline compounds than for the spinel lithium manganate, which gives an explanation for the greater initial discharge capacities of these nanocrystalline materials. On the other hand, I L_I-edge XAS spectra show that the iodine is stabilized as iodate species in the grain boundary or on the surface of the nanocrystalline manganese oxyiodide. Such an iodate species in the grain boundary is presumed to contribute to the maintenance of the nanocrystallinity of the present materials before and after Li insertion.

Acknowledgment. This work was supported in part by the Korean Ministry of Education (BSRI-99-3413) with the Brain Korea 21 fellowship for H. S. Park and by the Korean Ministry of Science and Technology through the National Research Laboratory Project (1999). C. W. Kwon thanks CROUS of Bordeaux in France for the financial support. Authors are also grateful to Prof. M. Nomura for helping us to get the XAS data in the Photon Factory.

References and Notes

(1) Thackeray, M. M. *Prog. Solid State Chem.* **1997**, *25*, 1.

(2) Armstrong, A. R.; Bruce, P. G. *Nature* **1996**, *381*, 499.

(3) Capitaine, F.; Gravereau, P.; Delmas, C. *Solid State Ionics* **1996**, *89*, 197.

(4) Koetschau, I.; Richard, M. N.; Dahn, J. R.; Soupart, J. B.; Rousche, J. C. *J. Electrochem. Soc.* **1995**, *142*, 2906.

(5) Hwang, S. J.; Park, H. S.; Choy, J. H.; Campet, G. *Chem. Mater.* **2000**, *12*, 1818.
(6) Gummow, R. J.; Liles, D. C.; Goodenough, J. B. *Mater. Res. Bull.* **1993**, *28*, 1249.
(7) Thackeray, M. M.; David, W. I. F.; Bruce, P. G.; Goodenough, J. B. *Mater. Res. Bull.* **1983**, *18*, 469.
(8) Treuil, N.; Labrugère, C.; Menetrier, M.; Portier, J.; Campet, G.; Deshayes, A.; Frison, J. C.; Hwang, S. J.; Song, S. W.; Choy, J. H. *J. Phys. Chem. B* **1999**, *103*, 2100.
(9) (a) Kim, J.; Manthiram, A. *Nature* **1997**, *390*, 265. (b) Manthiram, A.; Kim, J. *Chem. Mater.* **1998**, *10*, 2895. (c) Kim, J.; Manthiram, A. *Electrochem. Solid-State Lett.* **1999**, *2*, 55.
(10) (a) Jeong, Y. U.; Manthiram, A. *Electrochem. Solid-State Lett.* **1999**, *2*, 421. (b) Jeong, Y. U.; Manthiram, A. *J. Solid State Chem.* **2001**, *156*, 331. (c) Manthiram, A.; Kim, J.; Choi, S. *MRS Symp. Proc.* **2000**, *575*, 9.
(11) Xu, J. J.; Kinser, A. J.; Owens, B. B.; Amyrl, W. H. *Electrochem. Solid-State Lett.* **1998**, *1*, 1.
(12) Leroux, F.; Nazar, L. F.*Solid State Ionics* **1997**, *100*, 103.
(13) Chen, R.; Whittingham, M. S. *J. Electrochem. Soc.* **1997**, *144*, L64.
(14) Hwang, S. J.; Park, H. S.; Choy, J. H.; Campet, G. *J. Phys. Chem. B* **2000**, *104*, 7612.
(15) Hwang, S. J.; Park, H. S.; Choy, J. H.; Campet, G.; Portier, J.; Kwon, C. W.; Etourneau, J. *Electrochem. Solid-State Lett.* **2001**, *4*, A123.
(16) Considering the fact that the charge capacity for the first charge process (∼110 mAh/g) is much smaller than that for the following discharge process, the electrochemical activity of these electrode materials is considered to originate mainly from the insertion of lithium into the as-prepared nanocrystal. In this regard, we have probed the variation of the chemical bonding nature of nanocrystalline compounds before and after chemical lithiation reaction to understand the origin of its electrochemical activity.
(17) Oyanagi, H.; Matsushida, T.; Ito, M.; Kuroda, H. *KEK Report* **1984**, *83*, 30.
(18) Chen, R.; Zavalij, P.; Whittingham, M. S. *Chem. Mater.* **1996**, *8*, 1275.
(19) Kim, J.; Manthiram, A. *Electrochem. Solid-State Lett.* **1998**, *1*, 207.
(20) Kwon, C. W.; Campet, G.; Portier, J.; Poquet, A.; Fournes, L.; Labrugere, C.; Jousseaume, B.; Toupance, T.; Choy, J. H.; Subramanian, M. A. *Int. J. Inorg. Mater.* **2001**, *3*, 211.
(21) Campet, G.; Wen, S. J.; Han, S. D.; Shastry, M. C. R.; Portier, J.; Guizard, C.; Cot, L.; Xu, Y.; Salardennet, J. *Mater. Sci. Eng., B* **1993**, *18*, 201.
(22) Tsang, C.; Kim, J.; Manthiram, A. *J. Solid State Chem.* **1998**, *137*, 28.
(23) This material corresponds to the sample 2 in ref 22 with composition of $MnO_{1.89}$.
(24) Horne, C. R.; Bergmann, U.; Grush, M. M.; Perera, R. C. C.; Ederer, D. L.; Callcott, T. A.; Cairns, E. J.; Cramer, S. P. *J. Phys. Chem. B* **2000**, *104*, 9587.
(25) Hwang, S. J.; Park, H. S.; Choy, J. H.; Campet, G. *J. Phys. Chem. B* **2001**, *105*, 335.
(26) Horne, C. R.; Bergmann, U.; Kim, J.; Striebel, K. A.; Manthiram, A.; Cramer, S. P.; Cairns, E. J. *J. Electrochem. Soc.* **2000**, *147*, 395.
(27) Manceau, A.; Gorshkov, A. I.; Drits, V. A. *Am. Mineral.* **1992**, *77*, 1133.
(28) Inaba, M.; Iriyama, Y.; Ogumi, Z.; Todzuka, Y.; Tasaka, A. *J. Raman Spectrosc.* **1997**, *28*, 613.
(29) Jang, Y. I.; Huang, B.; Chiang, Y. M.; Sadoway, D. R. *Electrochem. Solid-State Lett.* **1998**, *1*, 13.
(30) Ammundsen, B.; Jones, D. J.; Rozière, J.; Villain, F. *J. Phys. Chem. B* **1998**, *102*, 7939.
(31) We have also tried to reproduce the experimental EXAFS data of lithiated derivatives on the basis of rhombohedral layered structure, but it gave poor fits and physically meaningless structural parameters.
(32) Hwang, S. J.; Park, N. G.; Kim, D. H.; Choy, J. H. *J. Solid State Chem.* **1998**, *138*, 66.